Mirror Coating Design for the Athena X-Ray Telescope

Bachelor's Thesis

Ida Flint Rasmussen
January 2017

Supervisor:
Desiree Della Monica Ferreira

DTU Space
National Space Institute

Abstract

The goal of this bachelor's thesis is to optimise the mirror coating for the X-ray telescope of the Athena mission, in order to obtain an improvement of reflectance at photon energies of 5 keV and above, without losses in the reflectance of energies below this. Coating optimisations are computed in the programme IMD, which uses the Fresnel equations to determine the reflectance of a multilayer structure. This reflectance is then applied to the geometry of the telescope, to obtain the effective area.
In this thesis, only bilayer structures have been optimised, but have been so in two different approaches. The first approach is testing various material combination, and optimising the recipes for these. The second approach is to divide the rings of mirror modules into a varying number of sections, and then, using the material combination from the first approach, which had the best performance, optimising the recipe for each section individually.

Contents

1 Introduction

Many larger scale structures in the Universe radiates almost exclusively photons in the X-ray range, which is only observable from space, since photons of these energies are absorbed by the Earths atmosphere. [7]
One such type of large scale structure is galaxy clusters, in which the intracluster medium (ICM) accounts for the majority of the clusters baryonic mass. Thus when examining the formation of these clusters of galaxies, the ICM is a vital part of understanding the development of the formation.
The ICM consists of hot gas, with a temperature, T, in the range of 2-14 keV, and is thin enough to be transparent to its own radiation. [7] At these temperatures the radiation emitted from the ICM will be almost exclusively in the form of thermal bremsstrahlung. Figure 1 shows the relative intensity of the photon energy emitted by thermal bremsstrahlung from a gas of temperature $T = 2 \times 10^8\,K \approx 17\,keV$. This temperature is a bit above the range of temperatures in the ICM, but it shows how the intensity decays exponentially with energy. Because of this and the distance to the galaxy clusters, a large throughput at lower X-ray energies is crucial for a telescope meant to observe these structures.

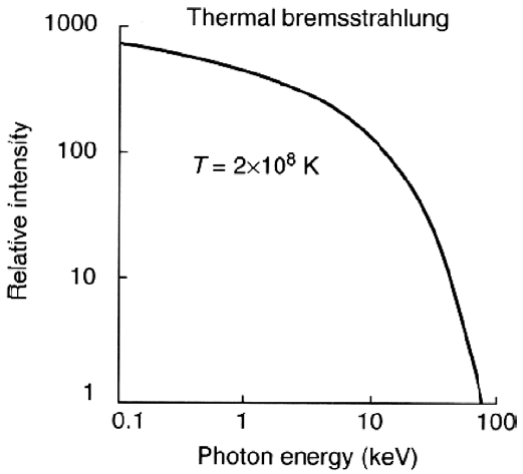

Figure 1: Spectral form expected from thermal bremsstrahlung in a hot gas at $2 \times 10^8\,K$. Thermal bremsstrahlung is characterised by the temperature of the gas, and at higher energies the intensity falls of exponentially.
Figure from (Seward and Charles, 2010). [7]

Observing galaxy clusters and their formation, along with black holes and neutron stars, are some of the scientific objectives of ESA's X-ray telescope Athena+. [1]
With the science objectives in mind, it is desired to obtain as large an effective area as possible for the telescope, especially in the lower energy range, where the thermal bremsstrahlung is most intense, in order to make better observations of the faint, distant

galaxy clusters.

Athena+ is set to launch in 2028, and will observe the sky in a low-energy X-ray range, from around 0.1 keV to about 10 keV. This is approximately the same energy range as the two currently functioning X-ray telescopes XMM-Newton and Chandra, which were both launched in 1999. This means that in 2028 XMM-Newton and Chandra will be ripe to be succeeded by a new telescope, which will apply some newer technologies in order to obtain a larger sensitivity, throughput and resolution, and therefore better observations.
The current baseline design for the Athena+ telescope, will give rise to an on-axis effective area (A_{eff}) of minimum 2 m^2 at 1 keV, and 0.1 m^2 at 8 keV. In Table 1 effective areas and angular resolution for the two current X-ray telescopes can be seen. It is clear that Athena+ will have a much larger effective area than both XMM-Newton and Chandra.

	Chandra	XMM-Newton	Athena+
Area @ 1 keV $[cm^2]$	800	1475	$2.33 \cdot 10^4$
Area @ 8 keV $[cm^2]$	100	580	$1.36 \cdot 10^3$
Angular resolution (HEW), [arcsec]	1	16	5

Table 1: Areas and angular resolutions are all on-axis. Values for Chandra and XMM-Newton are from (Willingale, 2002).[8] Values for Athena+ are from simulations and from (Ferreira et al., 2013).[3]

The purpose of this project is to try and improve the effective area of the Athena+ telescope in the higher part of its energy range, especially around 6 keV, where spectral lines for Fe are present, without causing losses in the lower energy range. This is done by computing the theoretical effective area of an array of viable material combinations (Ir/B_4C (base line material combination), W/Si, Pt/C, Ir, Ir/Si and Ir/SiC). The best candidate is then chosen for a second round of simulations, in which several recipes are used across the telescope, in order to improve the effective area further.

2 Theory & method

The wish is to determine the reflectivity of a number of material combinations of various thicknesses, when they are applied to the geometry of the Athena+ X-ray telescope, and then optimise the recipes for these material combinations in the energy bandwidth from 0.1 keV to 8 keV.

In the first part of this section, the geometry of the Athena+ telescope is explained, after which the methods used to find the projected area (A_{proj}) and the effective area (A_{eff}) of the telescope is described. Finally this section contains a description of the

programme used to compute these simulations of reflectace, and how the recipes were optimised.

2.1 Athena+ optics description

ESAs X-ray telescope Athena+ is a chonical approximation of the Wolter-I design, and alters at most from this approximation at the µm level. A Wolter-I telescope is a grazing incidence telescope, and consists of two mirrors; a primary mirror in the form of a paraboloid, and a secondary mirror in the form of a confocal and coaxial hyperboloid.[6] A schematic for this type of telescope can be seen in Figure 2.

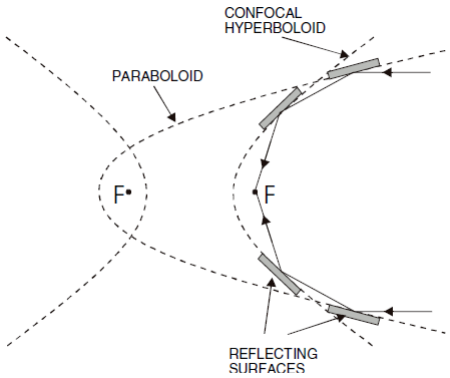

Figure 2: Illustration of a Wolter-I telescope. The focal point of the confocal hyperboloid is where the X-rays are focused and form the image.
Figure from (Reid, 2001). [6]

The Athena+ telescope has a focal length of 12 m, a radius of 1.5 m, and seen edge-on the telescope is comprised of 6 petals (see petal in Figure 4), each of which is filled with mirror modules (MMs).
These MMs individually consist of 70 Si plates, of which 68 of these are reflective mirror plates (MPs).[5]
The MMs are placed in 20 evenly radially spaced rows (or rings), and the width and length of the MMs (and thereby the number of MMs) in a row are optimised to decrease the area of unused space. [5]

The MPs are Si wafers replete with grooves, or "pores", to increase the effective area of the telescope. Each pore is 0.605 mm in depth and 0.83 mm wide, with a "wall" thickness of 0.17 mm, as is illustrated in Figure 3.

The surfaces of the Si wafers are coated with a high-Z material to reflect high energy photons, and a low-Z material as an overcoat to reflect lower energy photons. The current design for this coating is a 100 Å layer of Ir, topped with 80 Å of B_4C. This recipe

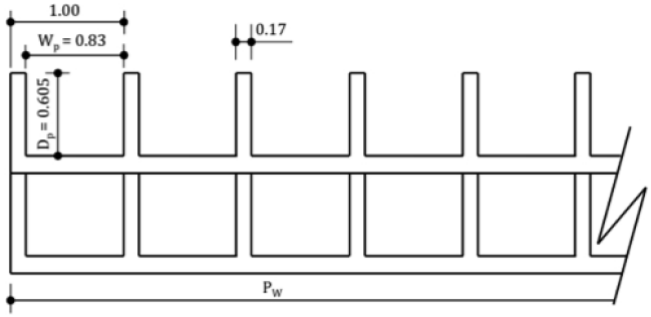

Figure 3: An illustration of the geometry of the pore structure in the mirror modules. P_w is the plate width, D_p is the pore depth and W_p is the pore width. All values in the figure are given in mm.
Figure from (Ferreira et al., 2012).[2]

is henceforth in this report called the baseline design.

2.2 Projected & effective area

The projected area (A_{proj}) is needed in order to determine the effective area (A_{eff}) of the telescope. A_{proj} is effectively calculated by summing the pore area for each row in the telescope.

First the number of MPs in a row is found by multiplying the number of MMs in the row by 68, since there are 68 reflective MPs in a MM.

$$n_{MP}(i) = 68 \cdot n_{MM}(i) \tag{1}$$

where i designates the specific row number in the telescope, i = 1 being the innermost row.
Then the number of pores in each MP can (approximately) be found by rounding the width of the MP (in mm) to an integer.

$$n_{pMP}(i) \simeq \frac{W_{MP}(i) - 0.17\,\mathrm{mm}}{1\,\mathrm{mm}} \tag{2}$$

where n_{pMP} is the number of pores in the MP of width W_{MP}.

The number of pores in each row of the telescope is then found by multiplying the number of pores per MP (n_{pMP}) with the number of MPs in the row.

$$n_p(i) = n_{pMP}(i) \cdot n_{MP}(i) \tag{3}$$

.

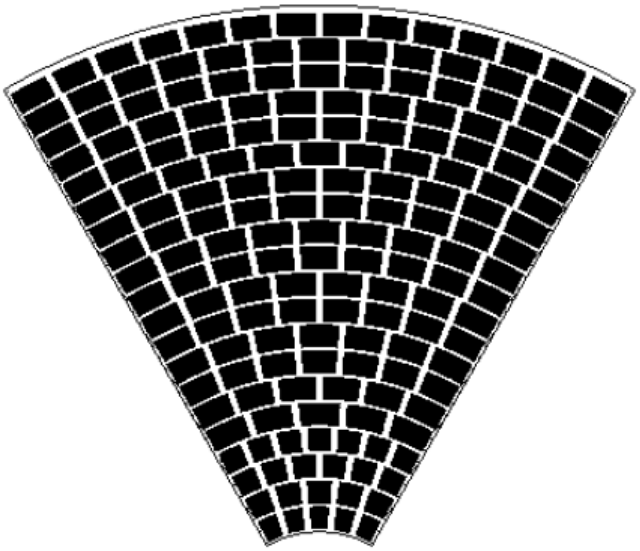

Figure 4: The layout of a petal in the Athena telescope. Each black box denotes a mirror module. Figure from (Oosterbroek, 2014).[5]

At last the projected area of each row can be calculated by

$$A_{proj}(i) = n_p(i) W_p D_p, \tag{4}$$

where W_p is the width of the pore, and D_p is the depth of the pore.

The total projected area can then of course be found by summing these individual areas

$$A_{proj,tot} = \sum_{i=1}^{20} A_{proj}(i). \tag{5}$$

All specific values for the Athena mirror used in the calculations above are from (Oosterbroek, 2014). [5]

The reason for creating an array with the areas of each row is, that every row has a specific grazing angle, α, for photons travelling with an on-axis trajectory. The grazing angles are needed in the calculations of the effective area.
Based on the focal length, F, and the middle radius, r of each row, the grazing angle, α, can be calculated as [5]

$$tan\,(4\alpha) = r/F \tag{6}$$

$$\Leftrightarrow \alpha = \frac{tan^{-1}\,(r/F)}{4} \tag{7}$$

Using the middle radius for each rows is of course an approximation. This approach is used since calculating the middle radius and grazing angle for every ring of MPs complicates the calculations to an extreme degree. It is thus assumed that the grazing angle does not vary significantly within a single ring, or that they will approximately even out to the grazing angle of the middle radius.

The effective area, A_{eff}, of a row can be described as a function of photon energy, E and the grazing angle, α. As each photon will be reflected twice, the on-axis effective area is dependent on the square of the reflectance, R.[3]

$$A_{eff} = \sum_{i=1}^{20} A_{proj}(i) \cdot R(E,\alpha)^2, \tag{8}$$

It is this reflectance from Eq. 8 which is computed in the programme IMD for all the various cases simulated.

2.2.1 IMD

For the reflectance simulations IMD is used. IMD is a programme run in the programming language IDL, which is capable of computing various (optical and) electromagnetic effects, such as reflectance, transmittance absorbtance, field intensity and more, for multilayer structures. [9]

2.2.1.1 FRESNEL function & Fresnel Equations

In this project IMD is used to simulate the average reflectance of bilayer structures in the energy range from 0.1 keV to 8 keV. This average reflectance is computed using the Fresnel-function in IMD, which uses the Fresnel equations in a recursion algorithm. [9]

By using the Fresnel equations the reflectance can be described as a function of the material, the angle of incidence and the polarisation of the light.
As the materials used in this project are non-magnetic, the reflection coefficient for light perpendicularly polarised to the plane of incidence can be described by [4]

$$r_s = \frac{n_i cos\theta_i - n_t cos\theta_t}{n_i cos\theta_i + n_t cos\theta_t}, \tag{9}$$

and the reflection coefficient for light polarised parallel to the plane of incidence is [4]

$$r_p = \frac{n_t cos\theta_i - n_i cos\theta_t}{n_i cos\theta_t + n_t cos\theta_i}, \tag{10}$$

where n_i is the refractive index on the incident side, n_t is the refractive index on the transmitted side, θ_i is the angle of incidence and θ_t is the angle of refraction.
The reflectivity of each type of light is then [10]

$$R_s = |r_s|^2 \tag{11}$$

and

$$R_p = |r_p|^2 . \tag{12}$$

The FRESNEL function can use these values to determine the average reflectance, R_{avg}, as [9]

$$R_{avg} = \frac{R_s Q(1+F) + R_p(1-F)}{F(Q-1) + (Q+1)}, \tag{13}$$

where Q and F are optional inputs in the function. Q is the polarisation analyser sensitivity, defined as the sensitivity to s-polarisation divided by the sensitivity to p-polarisation. F is the incident polarisation factor. It describes the incident intensities of the s-polarised light compared to the p-polarised light.
Here it is assumed that the instrument sensitivities to s- and p-polarisation are equal, and that the intensities of s- and p-polarised light are equal too. This means that the expression for the average reflectance can be shortened to

$$R_{avg} = \frac{1}{2}\left(R_s + R_p\right). \tag{14}$$

The required inputs for the FRESNEL function are the angle of incidence (θ), the energy of the light (λ), the optical constants for the materials at the given wavelengths (NC) and the thicknesses for the material layers (Z).

The input for angle of incidence must be a scalar or 1-dimensional array of incidence angles given in degrees, hence the used input is $\theta = 90° - \alpha$. Both θ and α are 1-dimensional arrays containing 20 values, one for each row of MMs.

The input for the wavelengths of photons, λ, is also a scalar or 1-dimensional array containing the wavelengths in the energy range desired to test reflectance within. It must be expressed in the same unit as the thicknesses of the layers in the structure, here that unit being Å. The range from 0.1 keV to 8 keV is used here with an increment of 0.1 keV between the values in the array. These energies are converted into Å before being used as input.

NC is a complex array of optical constants for the materials at the energies given in λ, and this array must be of the dimensions:
(number of elements in Z+2 , number of elements in λ).
IMD has a data base of optical constants for 150 materials. These constants are available for the energies spanning from the X-ray region to the infrared, more specifically from 0.124 Åto 3.33×10^6 Å, and comes from two laboratories; Center for X-Ray Optics (CXRO) and Lawrence Livernore National Laboratory.[9] In the simulations computed in this project, all optical constants used are from the latter mentioned laboratory, LLNL. For computing the optical constants a part of Desiree's code has been adapted and applied to the specific materials used.

Further, σ, an optional input, has been used. This input denotes the roughness of the interfaces between layers (including the top layer and the ambient medium). It can either be a scalar, a 1-dimensional array or a 3-dimensional array, and must also be in the same unit as λ and Z. [9]
In all but one simulation (the worst case scenario for the baseline design) a scalar of 4.5 Å has been used as roughness. In the worst case scenario a 1-dimensional array was used $\left[20\,\text{Å}, 4.5\,\text{Å}, 4.5\,\text{Å}\right]$, where the 20 Å is for the roughness of the boundary between the upper layer and the ambient medium.
The ambient medium used in the simulations is simply vacuum, as the mirror will be in space, where there is a near-vacuum. For the substrate, all simulations have used SiO.

Based on these inputs IMD can calculate the reflectance of the bilayer. This reflectance is then used in Eq. 8 to obtain the effective area of the telescope, when a specific recipe is used.

2.2.2 Optimising recipes

In all instances for both the multi-recipes and for the single recipe bilayer materials, the optimisation is computed by calculating the integrated effective area for thicknesses varying from 0-300 Å, in steps of 10 Å, for each layer. This integrated effective area is then stored in a 31x31-matrix, and the script identifies at which coordinates the maximum value for the integrated area lies, and will then prints the coordinates and the integrated effective area.

Of course this method does not take into consideration that it is our wish to preserve as much of the reflectance of the lower energies as possible, while adding to the effective area at higher energy levels. This is not a particularly big problem, since the consequence of thickening the high-Z layer typically will be, that more of the higher energy photons are reflected, but also that more of the lower energy photons are absorbed.

In the multiple bilayer recipe simulations this method of optimising has been used for each of the sections, and the script will, for each of these sections, print the coordinates for the maximum integrated effective area. Thus the best recipe for each of the

individual sections will be printed, starting from the innermost to the outermost section. Printed below the recipe description is the total integrated effective area, if this recipe combination were to be applied to the telescope.

The scripts for the multi-recipes bilayers will automatically save the optimised recipe combination in a data file called **"nrecipes.dat"**, where n = $[2, 4, 6, 8, 10]$ in correspondence to the number of sections which the rows have been split into.

3 Results from simulations

Two main types of simulations have been executed: One type for various material combinations, where the same layer thicknesses has been used for all rows in the telescope, and another type all using the same material combination, where the rows are split into a varying number of sections, each of which has their layer thicknesses optimised.

3.1 Single bilayer recipe

In the single-recipe simulations 7 material combinations have been tested: Ir/B_4C, the "worst case scenario" for Ir/B_4C, Ir alone, Ir/Si, Ir/SiC, W/Si and Pt/C.

All simulations have been performed in the energy range 0.1 keV-8 keV, and all with a interface roughness of 4.5 Å, with the exception of the worst case scenario for the base line.

	1 keV	3 keV	6 keV	8 keV	Integrated A_{eff}
Baseline, Ir/B_4C	2.33249	0.695237	0.259601	0.136267	66.996
Worst case for baseline	2.03870	0.657852	0.270544	0.142595	62.723
W/Si	2.08343	0.576441	0.222705	0.112353	55.987
Pt/C	2.13347	0.628277	0.236926	0.123350	62.347
Ir	1.83895	0.54862	0.256021	0.138693	56.532
Ir/Si	2.07760	0.587521	0.254713	0.135984	60.134
Ir/SiC	2.21338	0.631176	0.253755	0.133650	63.111

Table 2: The effective areas of material combinations at specific energies, and the integrated effective area. All areas are given in m^2.

3.1.1 Description of recipes

The following contains descriptions of the optimised recipes, and comparisons to the baseline.

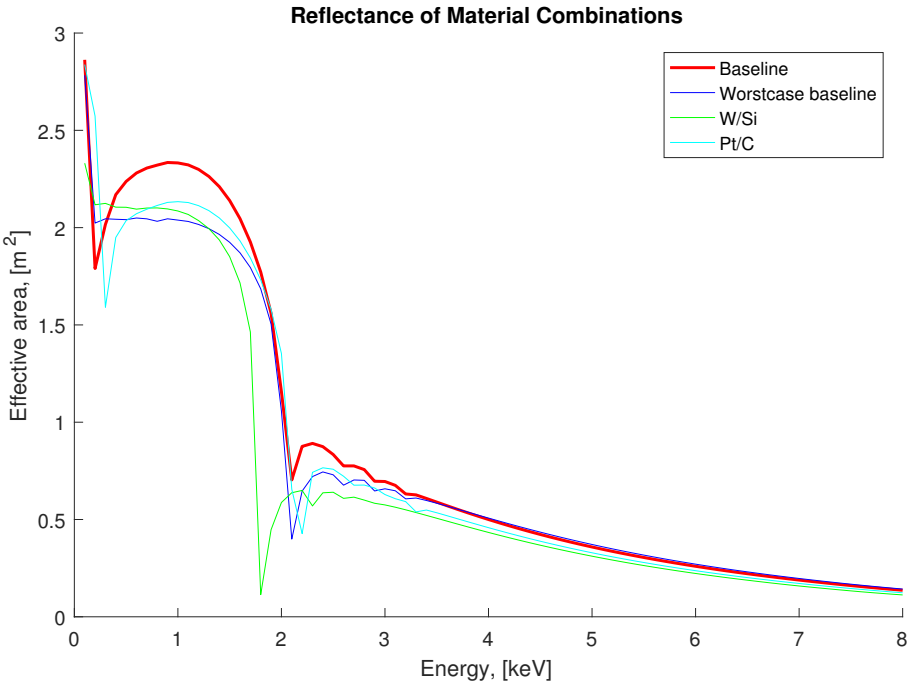

Figure 5: Effective area of the telescope as a function of photon energy.

3.1.1.1 Ir/B_4C

The Ir/B_4C bilayer is the current coating choice for the Athena+ optics. It consist of 100 Å of Ir, topped with 80 Å of B_4C.
For this material choice, a slight improvement was found for a change in the thickness of the B_4C layer from 80 Å to 70 Å. While the summarised effective area for the entire energy range was 67.0729 m^2 in contrast to the 66.9963 m^2 of the baseline. Over the entirety of the energy range, this is an improvement of only 0.0767 m^2.

All other results for the various material combinations and mutiple bilayer recipes are compared to the baseline design.

3.1.1.2 Worst case scenario for base line

Due to problems in the cleaning process of the MMs, there is at present a likely situation where most of the B_4C-layer is stripped from the mirror surfaces. For this reason, a simulation have been executed for a B_4C-layer of thickness Z =20 Å with a surface roughness of $\sigma = 20$ Å, while the parameters for the Ir-layer and the substrate have remained unchanged. This simulation is thought to give a reliable picture of performance of the Athena+ optics, if the upper layer of the coating is damaged on all MMs after

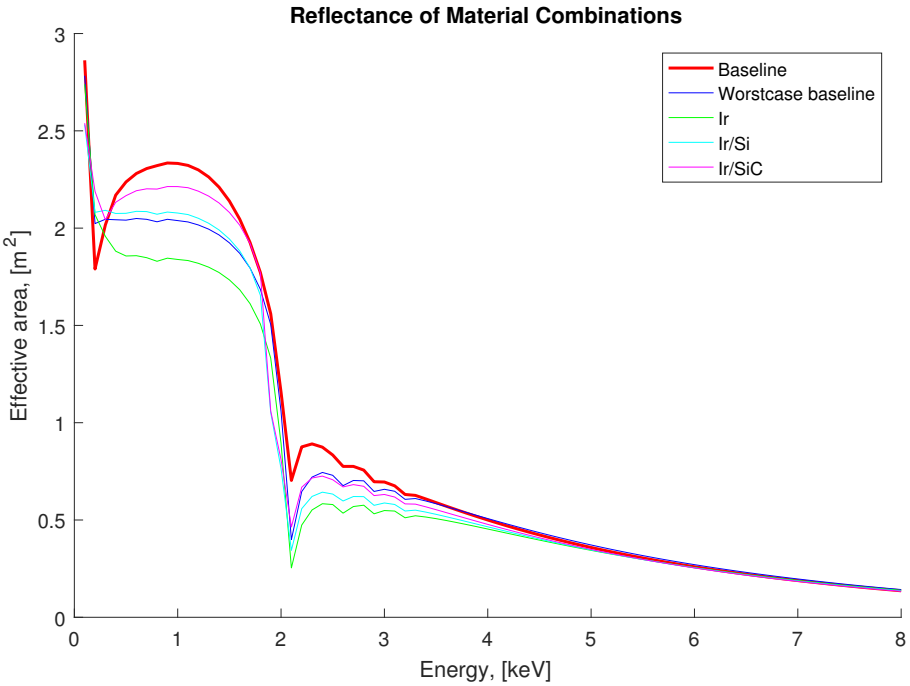

Figure 6: Effective area of the telescope as a function of photon energy.

being cleaned.

3.1.1.3 W/Si

The best performance in effective area for the material combination W/Si was found for 30 Å of Si on top of 120 Å of W.
As seen in Table 3, this material combination has the over-all worst performance, even when the worst case scenario baseline is taken into consideration. When compared to the baseline it has a loss of $\approx 10.6\%$ at 1 keV and a loss of $\approx 16.4\%$ in integrated effective area. Figure 5 reveals a great dip in effective area at around 1.8 keV, which isn't visible in Tables 2 and 3.
W/Si cannot be considered a good backup or alternative to the baseline design.

3.1.1.4 Pt/C

For this material combination, the best results were obtained from 60 Å of C on top of 100 Å of Pt. At the specified energies in Table 3 its performance is about a solid $8.5 - 9.5\%$ lower than that of the baseline. Its integrated effective area is below that of the worst case for baseline, but it maintains a bit more ($\approx 4\%$) of the effective area at 1 keV.

	1 keV	3 keV	6 keV	8 keV	Integrated A_{eff}
Worst case for baseline	87.404 %	94.623 %	104.22 %	104.64 %	93.622 %
W/Si	89.411 %	82.693 %	85.787 %	82.450 %	83.567%
Pt/C	91.467 %	90.369 %	91.265 %	90.521 %	93.061 %
Ir	78.841 %	78.911 %	98.621 %	101.78 %	84.381 %
Ir/Si	89.072 %	84.507 %	98.117 %	99.792 %	89.758 %
Ir/SiC	94.893 %	90.786 %	97.748 %	98.080 %	94.201 %

Table 3: The effective area for material combinations at specific energies, compared to the baseline.

It is not the worst of the material combinations, but it wouldn't be a good alternative to the baseline.

3.1.1.5 Ir

The optimised recipe for Ir calls for 110 Å of the material. As seen in Table 2 this coating yields the second smallest integrated effective area of all materials. Its performance is slightly above that of the baseline at 8 keV, but as seen in table 3 the effective area at 1 keV and 3 keV is roughly 20 % below baseline.
This simulation illustrates the importance of the low-Z top coating, when wanting to increase the effective area at the lower energy range. Even the worst case scenario for the baseline yields better results than Ir on its own.

3.1.1.6 Ir/Si

For this material combination the best results were obtained at 30 Å of Si on top of 110 Å of Ir. This yielded an integrated on-axis effective area of 60.134 m^2, which is $\approx$ 89.76% of the base line design. As seen in Table 3 and in Figure 6 it's performance is over-all lower than the base line (except in a tiny range from around 0.2 keV to 0.3 keV).
Again, the worst case for the baseline yields over-all better results than this material combination.

3.1.1.7 Ir/SiC

The best performance of the material combination Ir/SiC was found for 40 Å of SiC on top of 100 Å Ir. This recipe is the second best in performance, only after the baseline. It gives a slightly larger integrated effective area (94.2 % of baseline) than the worst case for baseline. It has its greatest loss of effective area, compared to baseline, at around 2 keV based on a reading of Figure 6.
Out of the tested material combinations, Ir/SiC is the best alternative to the baseline design, at least on paper.

3.2 Multiple bilayer recipes

As the baseline design still yields the best results out of the material combinations, it is used for the further simulations in the attempt to improve the reflectivity of the telescope. Below are descriptions of the optimised multiple bilayer recipes obtained in the simulations.
When looking at Figure 7 it becomes clear how similar the results for the varying number of sections are. It is along most of the graphs impossible to tell them apart. This gives evidence that this approach does not bring any vast improvements, neither compared to the baseline, nor among the multiple bilayer recipes themselves.

From Table 5 it is evident that all the multiple bilayer recipe simulations have losses at 1 keV and all but the results for the 6 sections simulation, have losses at 8 keV as well.

For the divisions of the rows of MMs the most staightforward method has been used. When possible each section contains the same number of rows each, otherwise the rows are as evenly distributed as possible.

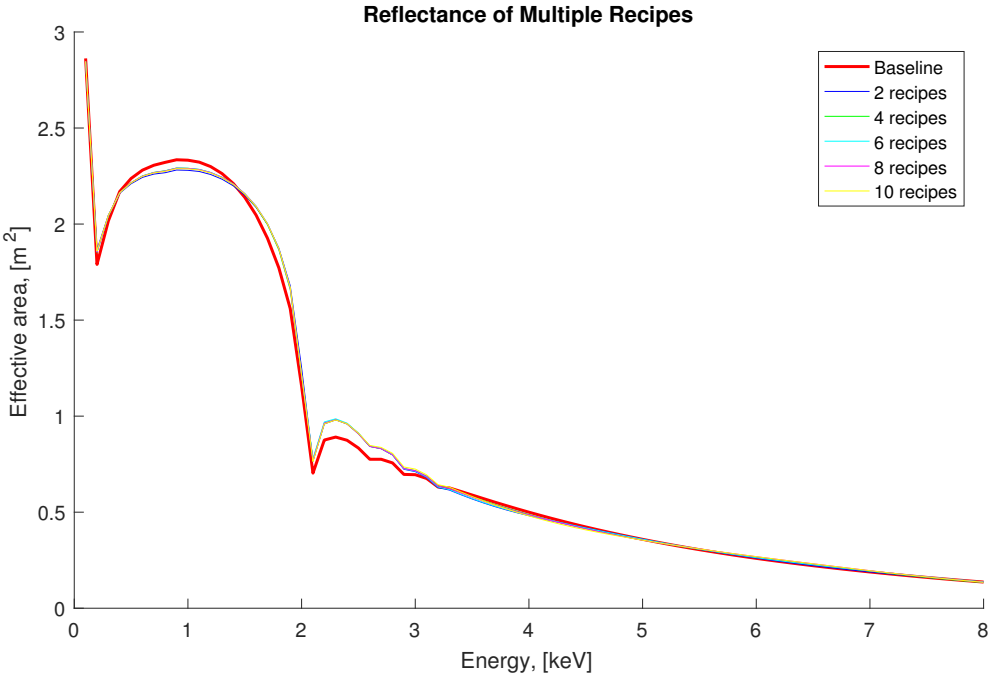

Figure 7: Caption

	1 keV	3 keV	6 keV	8 keV	Integrated A_{eff}
Baseline	2.33249	0.695237	0.259601	0.136267	66.9963
2 recipes	2.27980	0.711338	0.260740	0.135985	67.5317
4 recipes	2.29038	0.716578	0.265974	0.133467	67.7072
6 recipes	2.29012	0.713309	0.263386	0.137239	67.7364
8 recipes	2.28952	0.716090	0.268388	0.195484	67.7558
10 recipes	2.28732	0.724512	0.354402	0.134973	67.7594

Table 4: The effective areas for the multiple recipe designs at specific energies. All areas are given in m^2.

	1 keV	3 keV	6 keV	8 keV	Integrated A_{eff}
2 recipes	97.741 %	102.32 %	100.44 %	99.793 %	100.80 %
4 recipes	98.195 %	103.07 %	102.45 %	97.945 %	101.06 %
6 recipes	98.183 %	102.60 %	101.46 %	100.71 %	101.10 %
8 recipes	98.158 %	103.00 %	103.38 %	99.050 %	101.13 %
10 recipes	98.063 %	104.21 %	103.47 %	99.031 %	101.14 %

Table 5: The effective areas for the multiple recipe designs at specific energies, compared to basline.

3.2.1 Description of the section recipes

3.2.1.1 2 sections

Rows	B_4C [Å]	Ir [Å]
$1-10$	100	100
$11-20$	50	110

Table 6: Recipe description for telescope mirror divided into 2 sections.

For this simulation, the telescope was split into 2 sections, the first of which consists of the inner 10 rows and the second consisting of the 10 remaining outer rows.
The best results were obtained from the two thickness combinations seen in Table 6.
This recipe combination has an increased integrated effective area of 0.8 % compared to the baseline design, but as seen in Table 5 it has small losses at 1 and 8 keV.

3.2.1.2 4 sections

Rows	B_4C [Å]	Ir [Å]
$1-5$	120	120
$6-10$	90	90
$11-15$	60	80
$16-20$	50	140

Table 7: Caption

The mirror was split into 4 sections each containing 5 rings for this simulation. The thicknesses for the optimised recipes can be seen in Table 7.
Compared to the baseline design it has an increase of 1.06% in integrated effective area, but as for the majority of the simulations with the mirror divided into sections, the effective area suffers losses at 1 and 8 keV.

3.2.1.3 6 sections

Rows	B_4C [Å]	Ir [Å]
$1-4$	130	160
$5-8$	100	90
$9-11$	80	80
$12-14$	60	80
$15-17$	50	160
$18-20$	50	140

Table 8: Recipe description for 6 section simulation.

For this simulation, the telescope was split into 6 sections, the 3 inner of which each containing 4 rows, and the 3 outer each containing 3 rows. This choice of section division proved to obtain a larger integrated effective area than switching the simulation to have the 3 inner sections contain 3 rows each and the 3 outer sections consist of 4 rows each. This 6 section recipe has an increased integrated effective area of 1.1% compared to that of the baseline design. Out of the multiple section recipes, it is the only one not to suffer reflectance losses at 8 keV where it has an effective area of 100.7 % of that of the baseline. As seen in Table 5, it also has small improvements in effective area at 3 and 6 keV, while it suffers a loss of $\approx 1.8\%$ at 1 keV.

3.2.1.4 8 sections

Rows	B_4C [Å]	Ir [Å]
$1-2$	110	250
$3-4$	130	160
$5-6$	100	100
$7-8$	90	90
$9-11$	80	80
$12-14$	60	80
$15-17$	50	160
$18-20$	50	140

Table 9: Recipe description for the mirror divided into 8 sections

For this multiple bilayer recipe, the best results were found when the mirror was divided into 8 sections, the first 4 containing 2 rows MMs each, and the last 4 sections containing 3 rows each.
As for most of the other multiple bilayer recipes, this suffers from losses in effective area at 1 and 8 keV, but has a slight increase in integrated effective area of 1.13 % compared to the baseline.
At 3 and 6 keV it has an increase in effective area of 3.00 and 3.38 % respectively.

3.2.1.5 10 sections

Rows	B_4C [Å]	Ir [Å]
$1-2$	110	250
$3-4$	130	160
$5-6$	100	100
$7-8$	90	90
$9-10$	80	80
$11-12$	60	80
$13-14$	60	90
$15-16$	50	170
$17-18$	50	150
$19-20$	50	130

Table 10: Recipe description for the mirror divided into 10 sections

For this 10 section recipe, the mirror was divided into 10 sections each containing 2 rows of MMs. Out of the multiple bilayer recipe, this yields the largest integrated effective area at 101.14 % of that for the baseline, which makes it 0.01 percentage points larger than for the 8 section recipe.

As for the other multiple bilayer recipes, it suffers losses in effective area at 1 and 8 keV, while it gains 4.21 and 3.47 % at 3 and 6 keV respectively, when compared to the baseline design.

4 Discussion

4.1 Single bilayer recipe

As seen in Table 3 none of the material combinations' over-all performances are as good as the performance of base line design, and only one of these materials (Ir at 8 keV) has a better performance than Ir/B_4C at any of the specified energies shown in the table. From this it follows that the current base line design is still the best choice for coating the mirrors. This is only true however, as long as the B_4C-layer isn't remarkably damaged which seems to be the case in the present cleaning approach of the mirror plates after the coating has taken place.

In this case Ir/SiC seems to the best substitute for Ir/B_4C, since this material combination has the smallest loss of effective area at the lower energies (see Figure 6) and the second to largest integrated effective area at ≈ 94.2 % of the value for base line (see Table 2).
It does however have a smaller effective area in some energy ranges compared to the "worst case scenario" for base line, most notably from around 2.3 keV and up. In addition to being the second best over-all, after the base line it's the most reflective material combination at the lower energy range $\approx 0.5\,\text{keV} - 2\,\text{keV}$, yet its performance is below the base line and the "worst case scenario" at higher energies.

4.2 Multiple bilayer recipes

The second approach to optimising the on-axis effective area has been to split the rows of the telescope into sections, and optimising the Ir/B_4C recipe for each of these sections.

The results from these simulations show that there are small improvements of effective area at 3 and6 keV, but have not proven to contribute any large increases of the effective area. As seen in Table 4, 5 and Figure 7 there are barely any differences in the performance of these multiple bilayer recipes, and at 1 keV they all have a slightly smaller effective area than the base line design.
All the simulations using multiple recipes have slightly larger integrated on-axis effective areas compared to the baseline design ($100.80 - 101.14\%$ of baseline). However, when the extra work required in order to gain these small improvements of effective area is taken into consideration, the question arises if this is the best way to enhance the coating.
Using several recipes for the telescope requires the coating machine to be calibrated several times, but will at most, according to the results obtained in this project, increase the integrated effective area with 1.14%, while there are losses in effective area at 1 keV

for all multiple bilayer recipes.

There are of course other ways, than what have been used here, to split the mirror into the various number of sections, but based on the results obtained in this project, it is not likely to make much of a difference.

4.3 Future work

Since neither of the approaches discussed above have yielded any sizable improvements compared to the baseline design, it is questionable whether bilayers are the best way to go, when wanting to improve the effective area of Athena+.
A suggestion is to keep looking into multilayer coatings, as these seem to provide a somewhat larger effective area at the higher energies, without the effective area at the lower energies suffering as a result thereof. [3]

If there is not found any solution to the damage of the B_4C-layer in the baseline design, it might be reasonable to test the Ir/SiC recipe, to determine how this performs in practice since it's the best performing out of the tested alternatives to the baseline.

5 Conclusion

Out of the 5 alternative material combinations to Ir/B_4C none of them could improve the effective area at the higher energies, while still maintaining the effective area in the lower energy range.
If it proves impossible to use $Ir/B4_C$ for the coating, the best alternative found in this project is Ir/SiC. This material combination should however be tested in practice before concluding, that it actually is a viable alternative.

In the computations where the mirror rows were divided into sections, and different recipes of $Ir/B4_C$ were used on the individual sections, the 10 section recipe had the best performance in the range 3-6 keV, but the second greatest loss at 1 keV. The 6 section recipe is the closest of the tested recipes to fulfill the purpose of the project, as it has the second smallest loss at 1 keV ($\approx 1.8\%$) and is the only of the computations for several sections, which has increased the effective area at 6 and 8 keV with $\approx 1.5\%$ and 0.7% respectively.
As we still see a loss at 1 keV, none of the multiple section recipes really fulfill requirement of increasing the effective area of the telescope above 5 keV without the lower energy range of the telescope suffering as a result.

References

[1] Xavier Barcon, Didier Barret, Andy Fabian, Jan-Willem den Herder, Kirpal Nandra, Luigi Piro, and Mike Watson. The Hot and Energetic Universe - A White Paper presenting the science theme motivating the Athena+ mission. Technical report, ESA.

[2] D.D.M. Ferreira, F.E. Christensen, A.C. Jakobsen, N.J. Westergaard, and Brian Shortt. ATHENA optimized coating design. In Tadayuki Takahashi, Stephen S. Murray, and Jan-Willem A. den Herder, editors, *Proceedings of SPIE - The International Society for Optical Engineering*, volume 8443, page 84435L, sep 2012.

[3] D.D.M. Ferreira, F.E. Christensen, A.C. Jakobsen, N.J. Westergaard, and Brian Shortt. Coating optimization for the ATHENA+ mission. *Proceedings of SPIE - The International Society for Optical Engineering*, 8861:1–8, sep 2013.

[4] Eugene Hecht. *Optics*. Adison Wesley, 4th edition, 2002.

[5] Tim Oosterbroek. Athena telescope reference design and effective area estimates. 2014.

[6] Paul B. Reid. X-Ray Telescopes. In Paul Murdin, editor, *Encyclopedia of Astronomy and Astrophysics*, pages 1–10. Taylor & Francis, 2001.

[7] Frederick D. Seward and Philip A. Charles. *Exploring the X-ray universe*. Cambridge University Press, 2010.

[8] Richard Willingale. Grazing Incidence Optics. In Paul Murdin, editor, *Encyclopedia of Astronomy and Astrophysics*. Taylor & Francis, 2002.

[9] David L. Windt. IMD Version 5.0 - Installation Guide & User's Manual, 2013.

[10] Graham Woan. *The Cambridge Handbook of Physics Formulas*. Cambridge University Press, 2000.

DTU Space
National Space Institute
Technical University of Denmark

Elektrovej, building 327
DK - 2800 Kgs. Lyngby
Tel (+45) 4525 9500
Fax (+45) 4525 9575

www.space.dtu.dk